# Airborne time-domain electromagnetics, electrical resistivity and seismic reflection for regional three-dimensional mapping and characterization of the Spiritwood Valley Aquifer, Manitoba, Canada

Greg A. Oldenborger[*], André J.-M. Pugin and Susan E. Pullan

*Geological Survey of Canada, 601 Booth Street, Ottawa, Ontario K1A 0E8, Canada*

## ABSTRACT

The Geological Survey of Canada commissioned a helicopter-borne time-domain electromagnetic (HTEM) survey over a 1062 km$^2$ area of the Spiritwood Valley in southern Manitoba in order to test the effectiveness of airborne time-domain electromagnetics for mapping and characterizing buried valley aquifers in the Canadian Prairies. The data exhibit rich information content and clearly indicate the broader Spiritwood Valley in addition to a continuous incised valley along the broader valley bottom. We detect complex valley morphology with nested scales of valleys including at least three distinct valley features and multiple possible tributaries. Conductivity-depth images (CDI) derived from the HTEM decays indicate that the fill materials within the incised valleys are more resistive than the broader valley fill, consistent with an interpretation of sand and gravel. Comparison of ground-based electrical resistivity and seismic reflection data allow for the evaluation of CDI models. Lateral spatial information is in excellent agreement between data sets. However, CDI results tend to underestimate the dynamic range of electrical conductivity while overestimating depths to valley bottoms; these issues may be associated with system limitations, algorithm limitations or differences between data types. The integrated data sets illustrate that HTEM surveys have the potential to map complicated buried valley aquifers at a level of detail required for groundwater prospecting, modelling and management.

## INTRODUCTION

Buried valleys occur beneath the glaciated terrains of Canada, the Northern United States and Northern Europe, among other countries. When filled with coarse-grained permeable sediments, these valleys represent potential sources of groundwater. Productive buried valley aquifers are common in Canada, yet knowledge of their distribution and groundwater resource potential is inadequate (Russell *et al*. 2004; Betcher *et al*. 2005; Ahmad *et al*. 2009; van der Kamp and Maathius 2012). Systematic mapping and resource evaluation of buried valleys is hindered by complicated network geometries, the lack of surface expression and longitudinal and cross-sectional variability. At the regional scale, a complex buried valley system may form an aquifer. At smaller scales, components of the buried valley system may represent preferential flow paths that may have a significant influence on regional groundwater flow regimes, but may go unmapped or uncharacterized in traditional hydrogeological studies (e.g., Shaver and Pusc 1992; Abraham *et al*. 2010) especially in the absence of spatially

continuous data (Jørgensen and Sandersen 2009). Ground-based methods of subsurface investigation such as borehole coring and logging, pump tests, or ground geophysics provide localized information for conceptual model development but are not suitable for detailed regional mapping.

Airborne geophysics can provide rapid, high-resolution data acquisition at regional scales not achievable by ground surveys. Airborne electromagnetic (AEM) experiments are appropriate in groundwater exploration due to the dependence of electrical conductivity on water content and lithology (e.g., Palacky 1988). When tied to additional information such as high-quality boreholes, or ground geophysics, AEM surveys can be used to extrapolate knowledge to a regional scale, thereby capturing the complicated network of buried valleys as well as testing conceptual models.

Successful application of AEM to the mapping and characterization of buried valleys has been demonstrated in Germany (Gabriel *et al*. 2003; BurVal Working Group 2006; Steuer *et al*. 2009), Denmark (Auken *et al*. 2008; Jørgensen and Sandersen 2009; Siemon *et al*. 2009) and the United States (Smith *et al*.

[*] Greg.Oldenborger@NRCan.gc.ca

2010). Although the buried valleys may share a common morphology and origin, the geological context and the resulting electrical properties are different. Furthermore, depths of buried valleys across Canada will largely require time-domain AEM systems and commercial time-domain AEM instrumentation has been developed almost exclusively in a mineral exploration context (Fountain 1998; Allard 2007); see Sørensen and Auken (2004) for the notable exception of the SkyTEM system. Applicability of these systems for regional mapping of near-surface resistive materials has yet to be soundly established both in terms of target identification, data collection and processing (e.g., Martinez *et al.* 2008). Canadian commercial time-domain AEM systems have been utilized in groundwater studies for salinity mapping (e.g., Smith *et al.* 2004) and groundwater prospecting in arid environments (e.g., Wynn *et al.* 2005; Baldridge *et al.* 2007). However, these applications represent the detection/location of conductive targets in a variably resistive host with a strong contrast. We consider this to be distinct from the more general demands of resistivity mapping where the definition of the target and host become blurred, often with weak contrasts and/or the host being the more conductive material (e.g., Walker and Rudd 2008).

To test the applicability of airborne electromagnetics for the mapping and characterization of buried valley aquifers in Canada, the Geological Survey of Canada (GSC) carried out a helicopter-borne time-domain electromagnetic (HTEM) survey over the inferred region of the Spiritwood Valley Aquifer in southern Manitoba. The Spiritwood Valley Aquifer represents a municipal and rural source of groundwater (Wiecek 2009) and is trans-boundary with the state of North Dakota (Randich and Kuzniar 1984). The HTEM data were followed up with ground-based seismic reflection and electrical resistivity in order to better constrain the results in terms of structure and material properties (e.g., Jørgensen *et al.* 2003; Hoyer *et al.* 2011). This study represents one of the first applications of HTEM to aquifer mapping in Canada; the results demonstrate a significant value for regional three-dimensional aquifer mapping and characterization that may be applicable country-wide.

## THE SPIRITWOOD VALLEY

The Spiritwood Valley is a 15–20 km wide buried bedrock valley in southern Manitoba that runs approximately northwest-southeast near the towns of Killarney and Cartwright and extends 500 km from Manitoba, across North Dakota and into South Dakota (Winter *et al.* 1984). The current study area extends from the Canada-USA border to north-west of Killarney within a till plain of little topographic relief (Fig. 1). In this area, the bedrock valley has been identified and geographically constrained primarily based on water well information (Wiecek 2009) but its extent and character are poorly defined.

The stratigraphy within the valley is variable and includes basal sand and gravel, overlain by a series of undefined clay/silt till units locally interstratified with sand of variable thickness and extent. Basal sand and gravel are not observed throughout the valley. The underlying bedrock is fractured siliceous shale from the Odanah Member of the Pierre Formation (Randich and Kuzniar 1984).
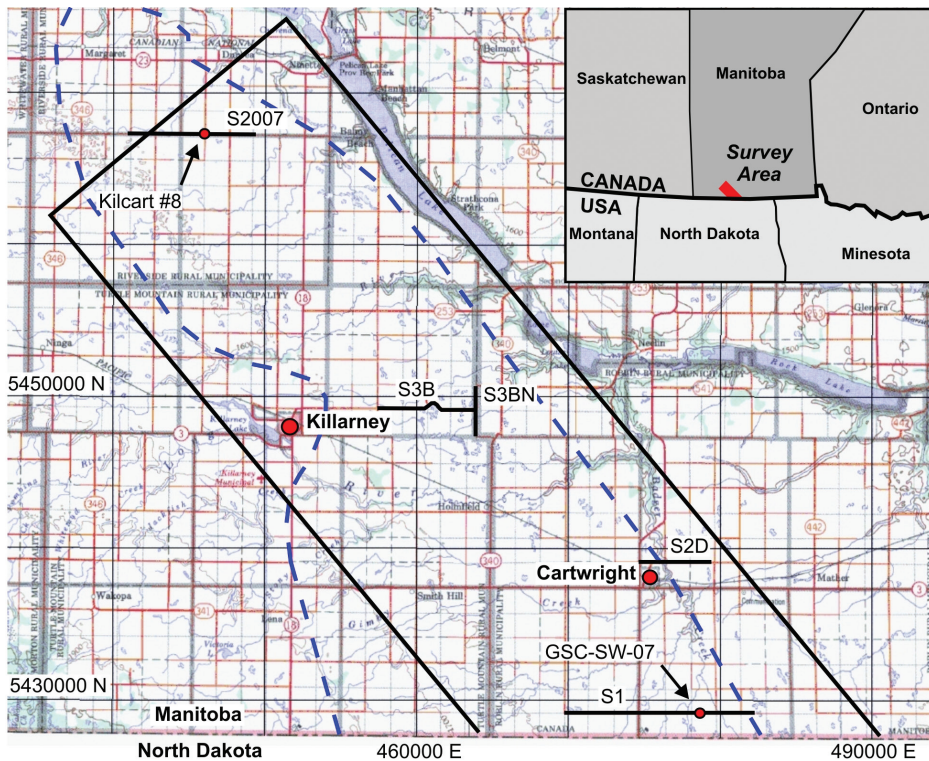


FIGURE 1

Spiritwood Valley Aquifer location map. The solid line indicates the 1062 km² HTEM survey block. The dashed line indicates the previous knowledge of aquifer extent (modified from Wiecek 2009). Also illustrated are the locations of the seismic reflection profiles (black lines) and electrical resistivity profiles (subsections of black lines) discussed in this paper and the Kilcart #8 and GSC-SW-07 boreholes. The inset map of Canada shows the survey area.
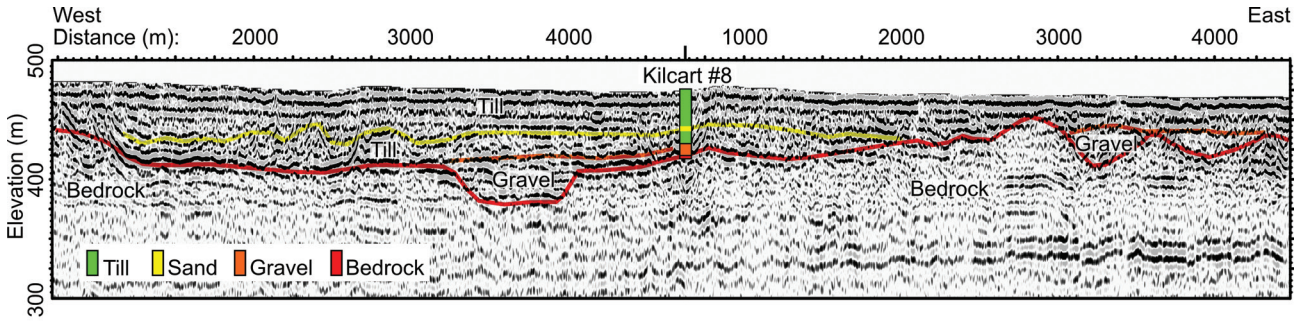
**FIGURE 2**

Interpreted P-wave seismic reflection section obtained north of Killarney, Manitoba (S2007). A simplified stratigraphic log for Kilcart #8 is illustrated for correlation. Vertical exaggeration: 8 times.
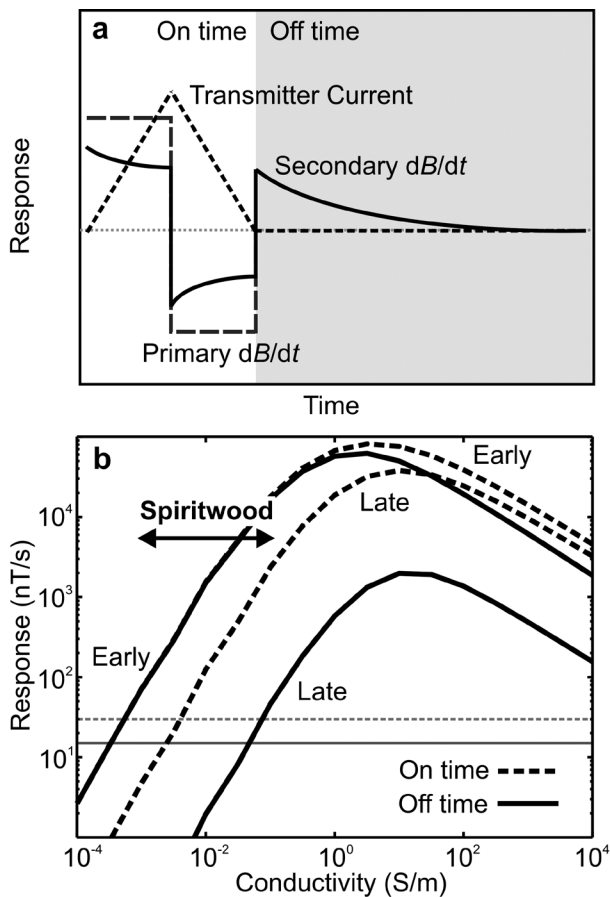


**FIGURE 3**

a) Schematic AeroTEM III transmitter waveform and response. At 90 Hz, the triangular current pulse is approximately 1.7 ms in duration. The on-time response is derived from both the up- and down-slope regions of the transmitter waveform. The duration of off-time measurements is approximately 3.4 ms after transmitter turn off. b) On-time and off-time half-space nomograms for the AeroTEM III system illustrating the conductivity range of the peak system response of the vertical component $dB_z/dt$ and the conductivity range expected for the Spiritwood Valley. The horizontal lines represent the approximate system noise levels. Provided by Aeroquest Surveys.

To better understand the valley morphology and fill, the GSC collected high-resolution landstreamer seismic reflection data north of Killarney near a local monitoring well with an occurrence of basal gravel (Fig. 1, S2007 and Kilcart #8). In addition to the broad valley architecture, the seismic data reveal a valley-within-valley morphology (Fig. 2; Pugin *et al*. 2009b; 2011). Within the broad Spiritwood Valley, we observe an incised valley approximately 800 m wide with a thalweg approximately 30 m below the bottom of the main valley. The incised valley extends from approximately 60–100 m depth and appears to be overfilled with up to 30 m of stratified sediments interpreted from the seismic facies as sand and gravel. The sand and gravel are observed to occur only within and directly adjacent to the incised valley. The continuity of the incised valley and of the basal sand and gravel are of significant interest for groundwater resource management in terms of groundwater access, flow and sustainability. Objectives for the HTEM survey include mapping the continuity of the incised valley and its fill material in addition to better defining the general geometry of the Spiritwood Valley Aquifer.

**HTEM SURVEY**

In near-surface investigations, airborne (dominantly helicopter) frequency-domain electromagnetic (FEM) systems are often employed on account of their large bandwidth and conductivity aperture, high-spatial resolution and strong response or discrimination capability within the shallow subsurface. FEM systems have been adapted for environmental and engineering applications including groundwater studies (e.g., Paterson and Bosschart 1987; Eberle and Siemon 2006; Meng 2006; Smith *et al*. 2010). However, as demonstrated by Steuer *et al*. (2009), FEM surveys have limited depth of penetration due to on-time measurement and system power limitations.

In contrast, airborne time-domain electromagnetic (TEM) systems are higher in power and offer increased depths of penetration. Design considerations for electromagnetic systems are complex (e.g., Palacky and West 1991; Allard 2007). However, in general, high power is achieved at the expense of early-time data and near-surface discrimination. This results in reduced bandwidth, limited conductivity aperture and a corre-

TABLE 1

Specifications for the AeroTEM III system.

| Data Rate (Hz) | Nominal Data Interval (m) | Base Frequency (Hz) | Pulse Width (ms) | Sample Frequency (kHz) | MTC[*] (m) | Loop Diameter (m) | Dipole Moment (Am²) |
|---|---|---|---|---|---|---|---|
| 10 | 2.3 | 90 | 1.7 | 36 | 35 | 9 | 237 000 |

[*]Mean Terrain Clearance

sponding deepening of response strength. Due to flight height and speed, fixed-wing TEM systems lack the spatial resolution necessary to detect small-scale targets. HTEM systems capitalize on the spatial resolution of the low-flying helicopter platform and the bandwidth is typically greater than for fixed-wing platforms.

The seismic reflection results and limited borehole data indicate depths of the Spiritwood aquifer of up to 100–120 m. The target depth requires a TEM system and the lateral scale of the incised valley requires an HTEM system. The system flown was a Canadian commercial system: the Aeroquest AeroTEM III (Balch *et al.* 2003). The AeroTEM system employs a rigid, concentric and bucked loop geometry with a triangular-bipolar current waveform (Fig. 3). The system measures voltage in an induction coil sensor, which is equivalent to the time rate of change of the secondary magnetic field d$B$/d$t$. Measured data are captured at a streamed rate of 36 kHz and are reported at a series of 16 constant-width time gates from 112.5–529.2 μs in the on-time and 17 variable-width time gates from 70.1–2917.3 μs in the off-time (Fig. 3). The system specifications are given in Table 1 (Oldenborger 2010a; 2010b).

**Electrical properties**

The geophysical logs for the Kilcart #8 borehole and a limited number of nearby boreholes provided an estimate of the expected electrical properties for the Spiritwood Valley during the planning stages. In general, the coarse materials representative of potential aquifers are resistive, the fine or poorly sorted materials are moderately conductive and the shale bedrock is conductive. The preliminary simplified electrical section consisted of three main units: till, 40–50 Ωm; sand and gravel, 70–200 Ωm; and shale bedrock, 5–50 Ωm (Oldenborger *et al.* 2010). The half-space nomogram for the AeroTEM III system response is illustrated in Fig. 3 and is representative of its conductivity aperture. The peak system response over a half-space occurs from approximately 1–10 S/m (1–0.1 Ωm) from early to late off-time. The system response falls below noise levels from approximately 0.001–0.1 S/m (1000–10 Ωm) from early to late off-time. The AeroTEM III waveform is designed to generate a strong response for high-conductance bodies (e.g., West *et al.* 1984; Smith and Annan 2000) and we see that the peak system response occurs for materials that are significantly more conductive than the Spiritwood Valley geology; this will be the case for most commercial HTEM systems. Nevertheless, the estimated electrical conductivities were deemed to be within the usable conductivity aperture.

**HTEM data**

The Spiritwood Valley HTEM survey block was aligned in the general direction of the mapped valley and is illustrated in Fig. 1. The traverse lines were planned at approximately 50° azimuth (cross-axis) with the control lines at 320° azimuth (along-axis). Survey geometry was designed based on a compromise between coverage and cost. Given the linear nature of the survey target and the estimated axial direction, traverse line spacing was set relatively high at 400 m. Further, since precise levelling of the magnetic data is of secondary concern, control lines were spaced at 5000 m. The survey consisted in a total of 2986 line km (Oldenborger 2010a; 2010b).

The survey and calibrations were flown during the period from February–March 2010. Data acquisition and processing were carried out by Aeroquest Surveys. The TEM decays were levelled for system drift using high-altitude corrections (e.g., Sørensen and Auken 2004) and converted to the parameters of apparent conductivity and decay constant (Oldenborger 2010a; 2010b). Conductivity-depth images (CDI) were generated from the TEM decays using the algorithm of Huang and Rudd (2008). The CDI models represent a time-dependent half-space conductivity fit to the individual TEM decays. For each decay, the time is translated to the effective depth using a calibrated diffusion depth.

**GROUND-BASED GEOPHYSICS**

To evaluate the performance of the HTEM survey, the GSC executed a ground geophysics campaign in the summer following airborne acquisition. The data consist in an additional 42 km of high-resolution landstreamer seismic reflection data (Pugin *et al.* 2011), in addition to more than 10 km of resistivity and induced polarization measurements collected along subsets of the seismic profiles. The locations of the illustrative profile lines are shown in Fig. 1. The seismic and electrical results will provide depth control (Jørgensen *et al.* 2003) and independent measurements of electrical conductivity.

**Seismic reflection**

The GSC near-surface seismic reflection methodology was described by Pugin *et al.* (2009a; 2009b). We utilize a three-component (3C) landstreamer receiver array and a Minivib vibratory seismic source. The landstreamer used for the Spiritwood Valley consisted of 48 3C geophones spaced at 1.5 m. The source was positioned 3 m from the nearest receiver and the mass was vibrated in the horizontal in-line direction with a non-linear (-2 dB/octave) sweep from 20–240 Hz (Pugin *et al.* 2011).

Even when vibrating the mass horizontally, 3C data provide both compressional-wave (P-wave) and shear-wave (S-wave) seismic sections (Pugin *et al*. 2009a). Most of the S-wave energy is generated within the first two seconds of the sweep (20–70 Hz), while the rest of the vibrating time contributes primarily to P-wave energy.

In many areas, particularly where the near-surface sediments are water-saturated or consist of dense till, good quality P-wave reflections are visible from overburden materials and bedrock. High amplitude P-wave reflections are indicative of coarse-grained material such as diamicton or sand and gravel. In areas of poor P-wave transmission, such as the central S3B section (Fig. 1), only S-wave reflection data are available. For low-velocity materials, S-waves usually provide higher resolution profiles with a wavelength four to five times shorter in comparison to P-wave data. Furthermore, the shear mode is not dependent on the nature of the porosity fill and good data do not depend on saturation. However, the shear mode is also less penetrative in complex and chaotic media such as course gravel or till.

### Electrical resistivity

We collected electrical and time-domain IP data along a subset of the seismic profiles using a Multi-Phase Technologies DAS-1 system. A 64-electrode array was used with modified dipole-dipole geometry. Dipole lengths ranged from 10–90 m and current dipoles were overlapped or circulated with 8 potential dipoles out to $n = 8$ (no fractional $n$ spacings). Surveys were performed at 1 Hz, 50% duty cycle with full reciprocals and rolled in sections of 32 electrodes.

Resistance data are filtered based on a combination of contact resistance, repeatability, reciprocal error and chargeability. After filtering and rejecting data outliers, the resistance data are inverted using the smoothness-constrained least-squares algorithm of Loke *et al.* (2003). The resulting electrical resistivity image (ERI) is a model of subsurface electrical resistivity. Model robustness is estimated using a depth of investigation methodology (Oldenburg and Li 1999; Oldenborger *et al.* 2007).

### RESULTS

The HTEM survey results are summarized in Figs 4 and 5 as the 3D CDI model of electrical conductivity interpolated to 100 m spacing in the north and east directions and 10 m spacing in depth. In the depth slices of Fig. 4, the geometry of the main Spiritwood Valley is readily apparent as a moderate conductivity feature (light blue/green) set amongst a conductive background (red) interpreted to be the response of the shale bedrock. The main valley is sinuous and approximately 8–10 km in width. In the centre of the main valley, we observe a continuous 1 km wide
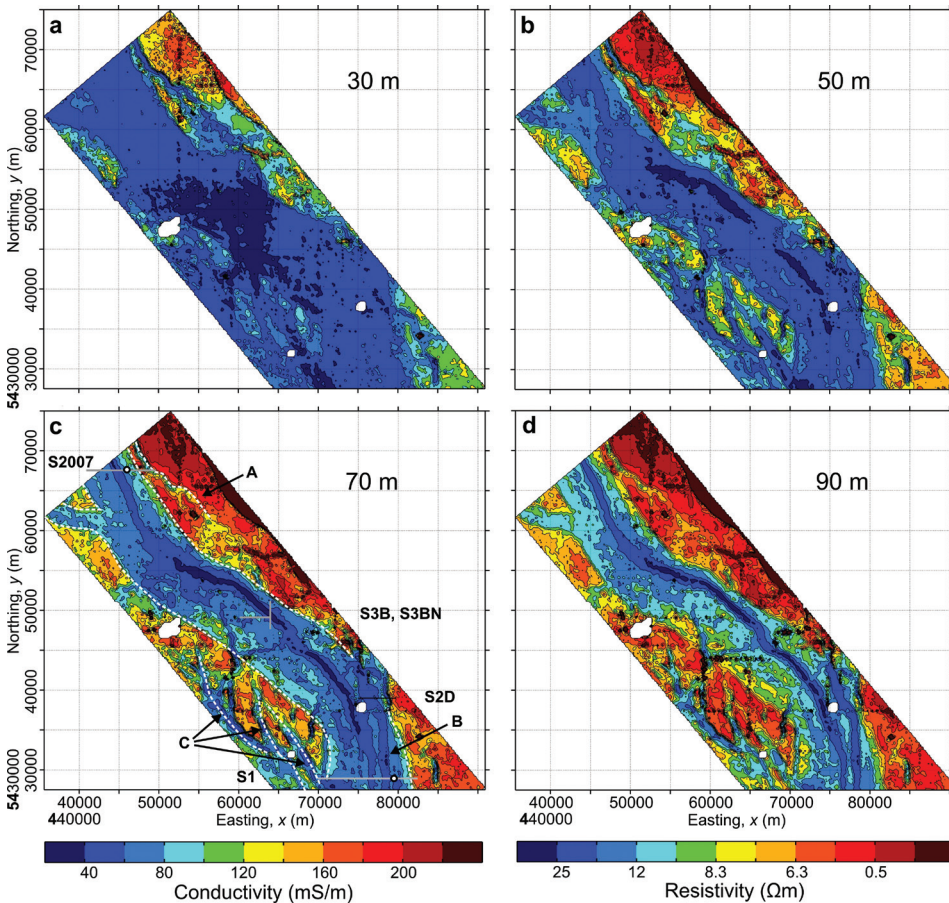


FIGURE 4

Depth slices of the 3D CDI model for the Spiritwood Valley survey block at a) 30 m, b) 50 m, c) 70 m and d) 90 m. Locations of the seismic and resistivity profiles are illustrated on the 70 m depth slice in addition to the interpreted boundary of the main Spiritwood Valley, narrow bedrock valley A, secondary incised valley B and a complicated valley network outside of the main valley C.
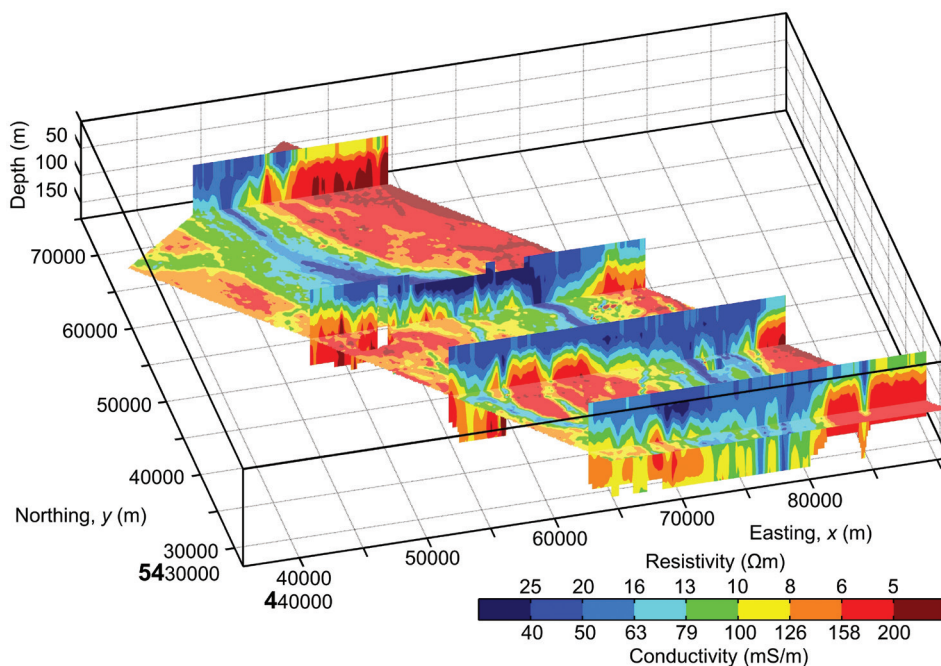
resistive linear feature (dark blue) that is interpreted as the incised valley identified in the initial seismic data (Fig. 2). In addition to the main and incised valleys, we also observe a narrow bedrock valley (Fig. 4c, A), a secondary incised valley (Fig. 4c, B) and a complicated valley network outside of the main valley (Fig. 4c, C), which may contribute to the previously mapped extent of the valley (Fig. 1).

The CDI model indicates that the narrow bedrock valley A may be a relatively shallow feature crossing the main Spiritwood Valley and joining the valley network C to the south (Fig. 4). The outside valley network C appears to have a strong shallow signature that disappears to the north and deepens to the south suggesting a dipping nature that is consistent with a USGS borehole 5 km south of the border that did not reach bedrock at 140 m (Randich and Kuzniar 1984). The secondary incised valley B is persistent with depth as much so as the main incised valley. Valley B may approach the surface as evidenced by its termination at bedrock (Fig. 4d, 5445000 N), although there may be some extension to the north-east as mapped by Betcher *et al.* (2005).

Also apparent from the CDI model is regional variability in the conductivity of the shallow valley fill along the valley axis. In particular, the central region near Killarney appears more resistive (Figs 4a and Fig. 5), indicative of a greater occurrence of inter-till sands in the area as noted by Wiecek (2009). At depth, the resistive signature of the incised valley is persistent. Figure 5 shows that the incised valley extends to the bottom of the CDI model, despite seismic data that indicate the deepest occurrence of bedrock to be approximately at 100 m depth. The extent of the incised valley at a great depth is a known artefact of the CDI algorithm that tends to image deep roots beneath resistive features (Huang and Rudd 2008).

**Profile S2007**

More insight into the performance of the HTEM survey can be gained by examining the CDI model shown in Figs 4 and 5 along the seismic and resistivity profiles located in Figs 1 and 4. Figure 6 illustrates an overlay of seismic, electrical and HTEM results along profile S2007. At the borehole location, the depth to bedrock is well resolved by the seismic data. Both the ERI and CDI models exhibit resistive anomalies that are well-aligned with the incised valley identified in the seismic data. The resistivity anomaly in the ERI model is imaged to extend above the interpreted gravel surface in the seismic data and it is not obviously seated on the interpreted bedrock surface. Repeated ERI synthetic modelling and inversion indicates that the true valley depth is consistent with the seismic data; placement of the anomaly slightly above the bedrock surface is likely a limitation of the smoothness constrained inversion. Modelling also indicates that the incised valley anomaly is consistent with erosion of both a supra-bedrock layer (till) and bedrock (Fig. 6b) and that the sand and gravel may extend above the interpreted seismic surface (Fig. 6a).

When we compare the CDI model to the ERI model, we see that shale appears more resistive and the valley fill appears more conductive; the CDI model exhibits a reduced dynamic range in comparison to the ERI model. This may be a function of the CDI imaging algorithm, or of improper system calibration, or of the difference between the two data types (induced horizontal currents versus galvanic vertical/horizontal currents). Preliminary 1D inversions (not shown) using the method of Faquharson and Oldenburg (1993) suggest that the inverted resistivity range from the HTEM data is more in agreement with the ERI models (approximately 5–50 Ωm). Regardless, the ERI models allow discrimination of the conductive basement, the resistive incised valley

fill, moderately resistive broad valley fill and overlying conductive till; whereas, for the CDI model, we are limited to discrimination of conductive bedrock and moderately resistive overburden, with isolated regions of high resistivity. The depth to bedrock is well constrained by both the ERI and CDI models over the profile. However, we note that based on the interpreted seismic surface, the bedrock interface may be multi-valued in terms of resistivity for either the ERI or CDI model and that due to model smoothness, the resistivity at that interface may be significantly more resistive than the true shale resistivity. Furthermore, the CDI model exhibits a resistive root associated with the incised valley but not with the smaller eastern bedrock valley.

### Profiles S3BN and S3B

The S-wave data acquired along profiles S3BN and S3B are illustrated in Figs 7 and 8 respectively. The shallow data are high reso-

lution with a central frequency of about 55 Hz. Below a high-amplitude reflection surface at approximately 450 m elevation, the frequency content drops dramatically to 35 Hz. This hard interface is interpreted to be the top of a dense till. In order to present both spectra in the same section, a time-variant band-pass filter was used during the processing to show these two very different wavelengths in the same section and a variable interval velocity model was used for depth conversion (e.g., Pugin *et al.* 2009b).

We observe two valleys in the seismic profiles, the targeted central incised valley along profile S3BN interpreted to be gravel-filled (Fig. 7) and a shallow valley along profile S3B, also interpreted to be gravel-filled (Fig. 8). The ERI model clearly captures the deep valley and bedrock topography (Fig. 7a) and the high-resistivity anomaly suggests coarse valley fill and potential aquifer material consistent with the seismic data. The CDI model also captures the deep valley, places
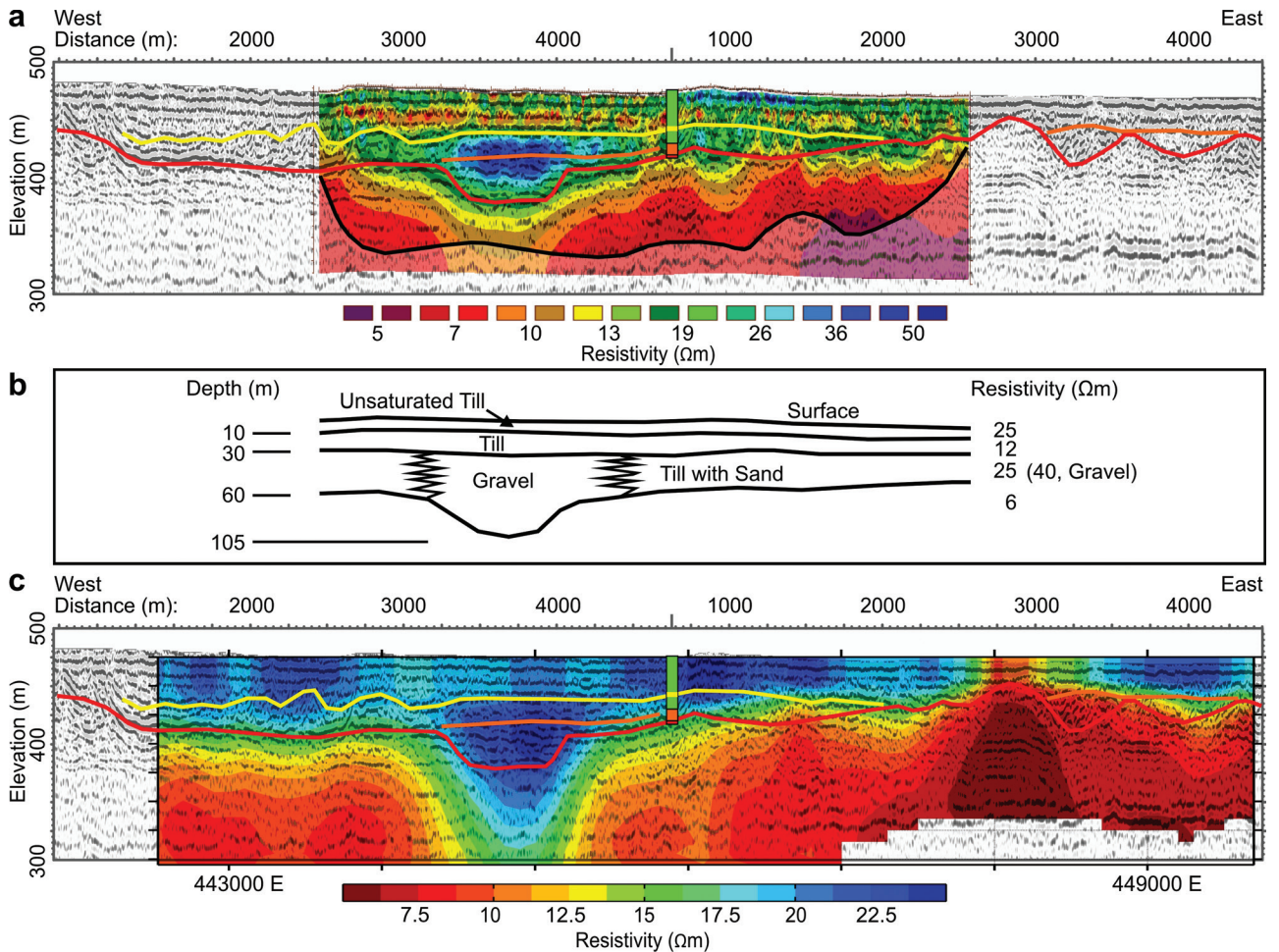


FIGURE 6

Comparison of HTEM, seismic and ERI results for profile S2007. a) ERI model overlain on an interpreted seismic section. The solid black line indicates the approximate depth of investigation below which the model is heavily influenced by regularization. b) Schematic interpretation of the ERI model based on repeated synthetic modelling and inversion. c) CDI model overlain on an interpreted seismic section. Different colour scales are used to illustrate the different ranges in model values. A logarithmic colour scale for the ERI model accentuates discrimination of low-to-mid-range resistivities. A linear scale for the CDI model accentuates discrimination over the smaller range of values.
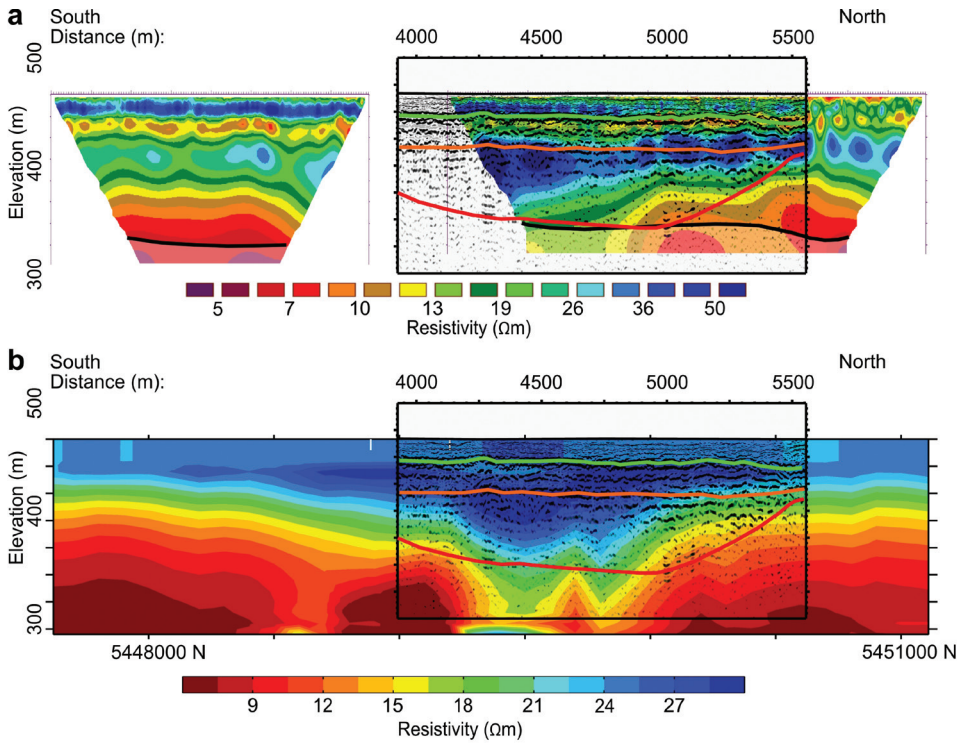
FIGURE 7

Comparison of HTEM, seismic and ERI results for profile S3BN. a) ERI model overlain on an interpreted S-wave seismic section. b) CDI model overlain on an interpreted seismic section. Inter-till boundaries are green, gravel surface is orange and bedrock surface is red.
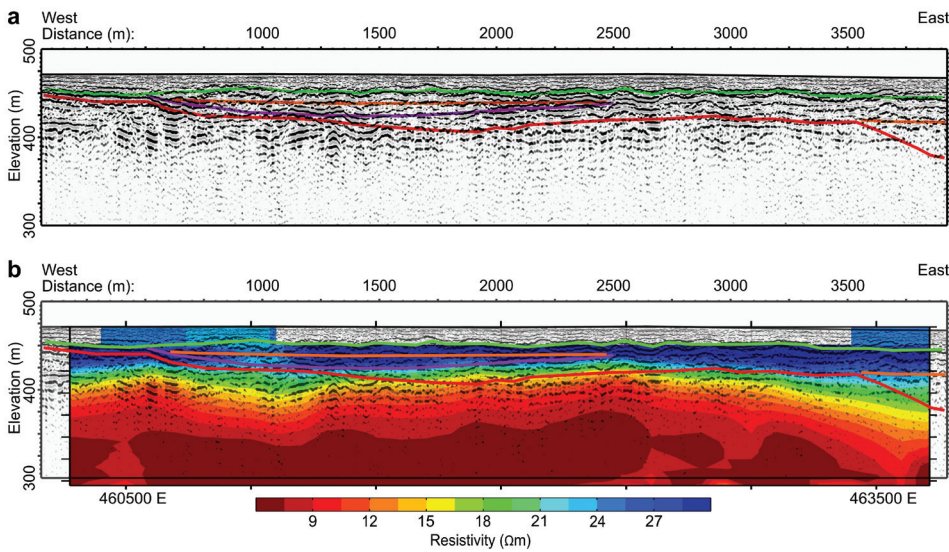


FIGURE 8

Comparison of HTEM and seismic results for profile S3B. a) Interpreted S-wave seismic section. Inter-till boundaries are green, gravel surface is orange, bedrock surface is red and erosional surface is purple. b) CDI model overlain on an interpreted seismic section.

it in a consistent location with the ERI model and extends the knowledge of bedrock topography beyond the ground data (Fig. 7b). However, both the CDI and ERI models suggest that the valley does not extend as far north as interpreted in the seismic section. The CDI model depicts a less resistive overburden generally reflective of overlying tills. But the ERI model exhibits a more complicated near-surface with a transition from the valley fill to the overlying till to a resistive surface material above the hard reflection surface identified in the seismic data. This resistive surface layer extends to the south and east (not shown) and may be associated with a high occurrence of

inter-till sands in the Killarney region (Wiecek 2009; Fig. 4a).

Along profile S3B, the shallow valley is marked by an erosional surface in the seismic data (Fig. 8a, 500–2500 m distance). Despite good bedrock topography, the shallow valley is not readily apparent in the CDI model in Fig. 8(b). By using depth-independent colour scales, the shallow valley can be observed in the CDI depth slices as a linear feature trending north-south and intersecting the central incised valley to the north (Fig. 9). Such channel intersections potentially provide vertical hydrologic windows, which could be critical recharge zones that affect the long-term sustainability of groundwater resources.

**Profile S2D**

The target of profile S2D was the secondary incised valley B indicated in Fig. 4. The interpreted P-wave seismic section identifies the valley and suggests coarse fill at a depth associated with high-amplitude reflections (Fig. 10). The ERI model recovers some hint of the valley as a break in the electrical structure from 1000–2000 m distance but there is no resistive anomaly. The seismic surfaces at approximately 10 m and 30 m depth are well

recovered by the ERI model as the top and bottom of a conductive layer (till) but resistive material is found on the valley flanks and the valley is actually relatively conductive. Although complicated, the ERI model supports the seismic interpretation that the incised valley is a post-till erosional feature.

Similarly, while the CDI model recovers the valley structure observed in the seismic data for profile S2D, the resistivity of the valley fill is less than that observed for the primary incised valley
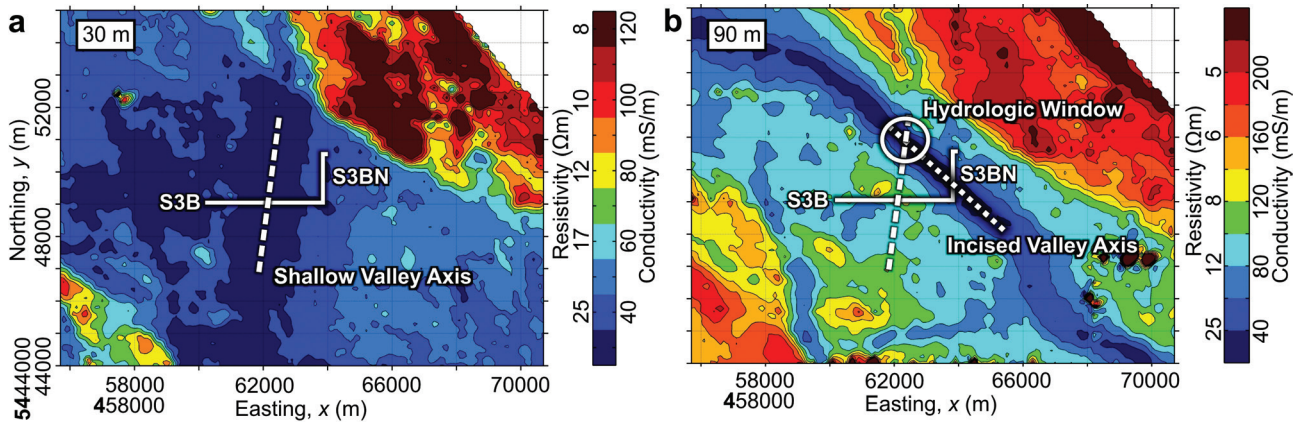


FIGURE 9

Joint interpretation of seismic data and the CDI model illustrating the relationship between erosional features. a) CDI at 30 m depth with a shallow valley axis interpreted from profile S3B (Fig. 8). b) CDI at 90 m depth with an incised valley axis interpreted from profile S3BN (Fig. 7). The shallow valley is observed to intersect the deeper incised valley; the result is a potential hydrologic window.
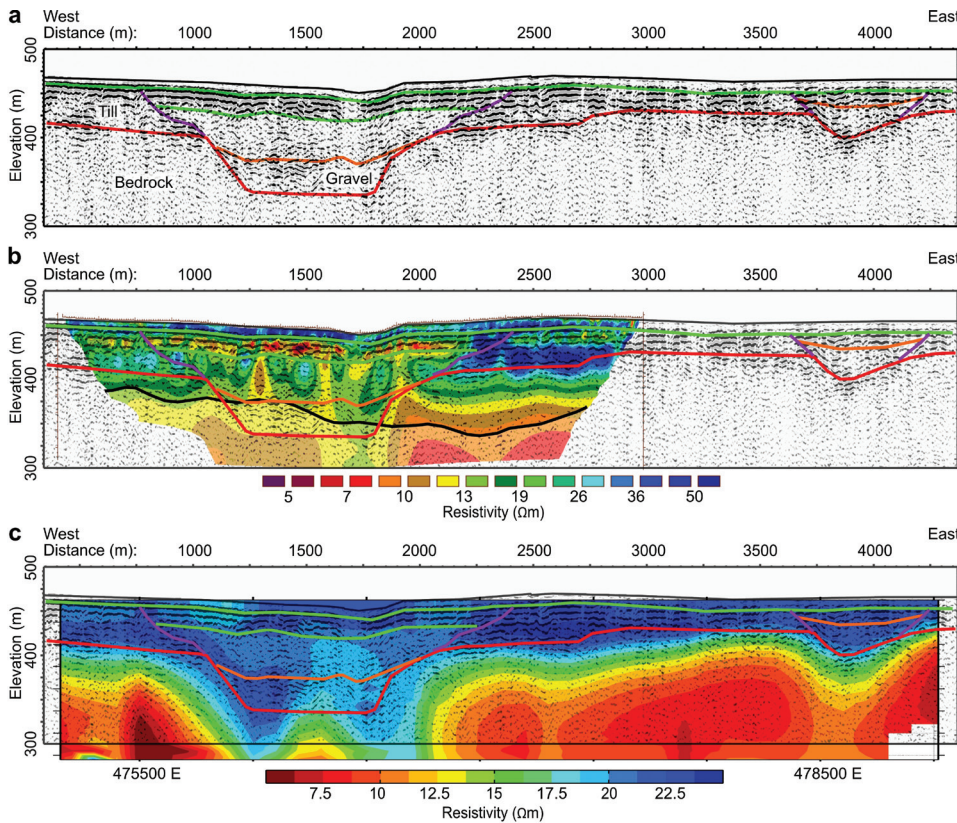


FIGURE 10

Comparison of HTEM, seismic and ERI results for profile S2D. a) Interpreted P-wave seismic section. Inter-till boundaries are green, gravel surface is orange, bedrock surface is red and erosional surfaces are purple. b) ERI model overlain on an interpreted seismic section. c) CDI model overlain on an interpreted seismic section.

(e.g., Fig. 7) and is less than the resistivity of the material on the valley flanks. These observations from both the ERI and CDI models may indicate a change in valley fill such as increased shale provenance, inflow of conductive water from the shale bedrock to the valley, or infiltration of conductive surface water from Badger Creek at a 1750 m distance; these hypotheses are untested.

**Profile S1**

The P-wave seismic section along profile S1 can be interpreted in terms of details about the valley features and the internal sequential stratigraphy of the valley fill (Fig. 11a). The main incised valley (western) and the secondary incised valley (eastern) are observed in the seismic data as infilled valleys cut into bedrock to depths in excess of 100 m below ground surface. The high-amplitude character of the incised valley reflections suggest that the sedimentary fill is coarse-grained sand in the western valley and coarse gravel overlain by till in the eastern valley.

A GSC borehole was completed on profile S1 after the ground geophysics campaign (Crow *et al.* 2012). Results for GSC-SW-07 (Figs 1 and 4) are illustrated on the seismic section as a simplified stratigraphic log. The strong inter-till reflectors observed in the seismic data correlate with sections of no recovery in the borehole core. These no recovery sections are often observed to be associated with cobble-rich units or sands and above and below the no recovery zones there are differences in till geochemistry. These observations indicate that, within the thick till package, the seismic data are sensitive to distinct depositional units. Beneath the till, the borehole log indicates that the gravel units occur deeper than the surface interpreted as the top of the gravel seismic facies. Furthermore, while gravel is observed in the borehole log, there is an equal or more abundant amount of sand and a significant occurrence of inter-gravel till.

The CDI model is consistent with the seismic interpretation and shows resistive anomalies in both valleys (Fig. 12b). However, in addition to the secondary incised valley having reduced resistiv-

ity as along profile S2D (Fig. 11), the main incised valley also exhibits a weakened resistive signature along profile S1. From Fig. 5, we see increased conductivity of the main valley fill as we move southward from S2D to S1 with a reduced distinction in conductivity between the fill of the main and incised valleys. This may indicate significant variability in either valley fill or pore water characteristics down the valley axis.

ERI models for other profiles (Figs 6 and 7) indicate that the inter-till surfaces identified in the seismic data are associated with contrasts in electrical resistivity. For profile S1, the CDI model is not able to discriminate the variability in the till overburden that is observed in the seismic data, although there is some indication of near-surface heterogeneity. For profile S1, the CDI model exhibits very pronounced resistive root artefacts beneath the valleys. Nevertheless, this southernmost extent of our survey suggests that two significant valley features cross the international border within the main Spiritwood Valley and that there may be limited hydraulic connection between them.

**CONCLUSIONS**

Helicopter-borne TEM data were collected over the Spiritwood Valley Aquifer in southern Manitoba in order to test the applicability for mapping and characterizing buried valley aquifers in the Canadian prairie landscape. The ultimate goal of the geophysical imaging applied to the regional groundwater mapping is the accurate placement of information in 3D, a reliable characterization of the electrical and material properties of the valley fill sediments and an improved understanding of the aquifer system. In terms of improved understanding, the HTEM data over the Spiritwood Valley Aquifer have thus far provided, for the first time, a sense of the full buried valley geometry, the variability of valley orientation and fill material, the complexity of multiple valley relations and stratigraphic nesting of valleys.

The combination of the HTEM data with seismic reflection data and electrical resistivity surveying has allowed us to evalu-
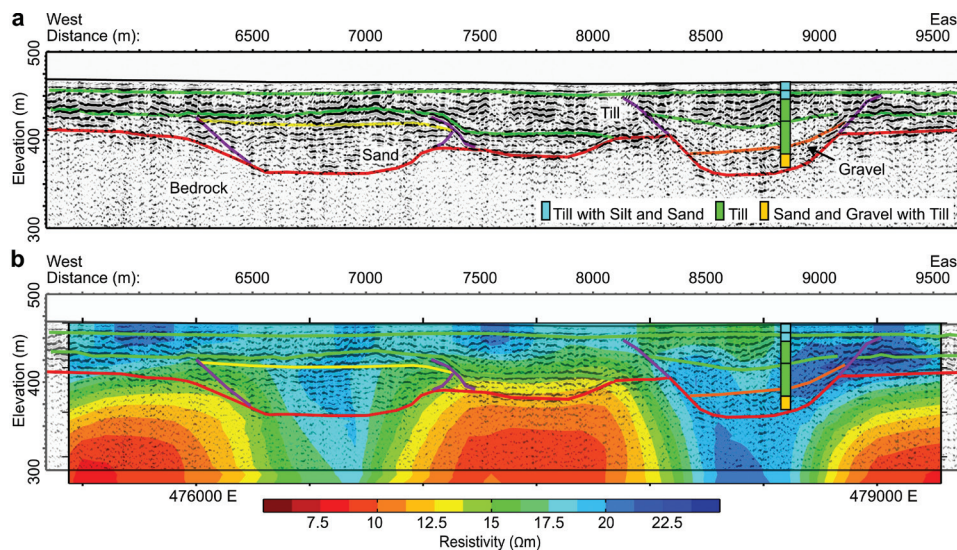


FIGURE 11
Comparison of HTEM and seismic results for profile S1. A simplified stratigraphic log for GSC-SW-07 is illustrated for correlation. a) Interpreted P-wave seismic reflection section. Inter-till boundaries are green, sand surface is yellow, gravel surface is orange, bedrock surface is red and erosional surfaces are purple. b) CDI model overlain on an interpreted seismic section.

ate the HTEM data in terms of lateral spatial control and depth information. The valley features interpreted from the CDI model are in agreement with valley features interpreted from the seismic reflection and ERI. In general, near-surface resolution of the CDI model is limited, likely due to early-time limitations of the AeroTEM system that can be both system and bandwidth related (Macnae and Baron-Hay 2010). We find the earliest useable time to be approximately 100 µs. The conductive bedrock surface is well resolved by the CDI model over the main Spiritwood Valley. For some transects across the incised valley (S3BN) the depth of the incised valley is also in good agreement with the supporting data. However, for other transects across the incised valley (S2007 and S1), we observe deep resistive roots. As such, additional information (seismic) will be required to control depth estimates of the incised valleys for 3D geological modelling.

Within the Spiritwood Valley, the electrical resistivity obtained from the CDI model is underestimated and of reduced range when compared to the ERI models. Much of the reduced range appears attributable to the CDI algorithm; it is unclear how much may also be due to the conductivity aperture of the AeroTEM system but this is a current subject of investigation. The implication is that material property estimation based on CDI results alone will likely be of poor fidelity without some kind of supporting information. The practical consequence is that discrimination of aquifer materials is hampered. Nevertheless, we observe a marked difference in material properties between the fill in the main and incised valleys. The incised valley fill is more resistive, consistent with coarse-grained aquifer material. The main valley fill exhibits significant variability, with high-resistivity zones perhaps indicative of inter-till sands. The incised valley fill is also variable with highest resistivity in the central survey region and reduced resistivity southward. Despite the early-time limitation and despite the fact that the AeroTEM system is not designed for a peak response over resistivities such as those found in the Spiritwood Valley, the AeroTEM data are rich in information content and do provide detailed lithological identification. More resistive aquifer scenarios such as granitic/fluvial sand and gravel, or igneous bedrock will be further from the peak response of the AeroTEM system; such scenarios may require alternative systems or methods.

Our results suggest that HTEM surveys have the potential to map buried valley aquifers in the Canadian Prairies in great detail over large areas. The HTEM data successfully map valley locations that continue to be difficult to define using seismic and borehole methods. Our observations improve understanding of the spatial variability of valley fill that has complicated the positioning of groundwater monitoring wells and hydraulic modelling of buried valley aquifers.

## ACKNOWLEDGEMENTS

## REFERENCES

Abraham J.D., Cannia J.C., Peterson S.M., Smith B.D., Minsley B.J. and Bedrosian P.A. 2010. Using airborne geophysical surveys to improve groundwater resource management models. *Proceedings of the Symposium on the Application of Geophysics to Environmental and Engineering Problems*, pp. 309–314.

Ahmad J., Schmitt D.R., Rokosh C.D. and Pawlowicz J.G. 2009. High-resolution seismic and resistivity profiling of a buried Quaternary subglacial valley: Northern Alberta, Canada. *GSA Bulletin* **121**, 1570–1583.

Allard M. 2007. On the origin of the HTEM species. *Proceedings of the Fifth Decennial International Conference on Mineral Exploration*, pp. 355–374.

Auken E., Christiansen A.V., Jacobsen L.H. and Sørensen K.I. 2008. A resolution study of buried valleys using laterally constrained inversion of TEM data. *Journal of Applied Geophysics* **65**, 10–20.

Balch S.J., Boyko W.P. and Paterson N.R. 2003. The AeroTEM airborne electromagnetic system. *The Leading Edge* **22**, 562–566.

Baldridge W.S., Cole G.L., Robinson B.A. and Jiracek G.R. 2007. Application of time-domain airborne electromagnetic induction to hydrogeologic investigations on the Pajariti Plateau, New Mexico, USA. *Geophysics* **72**, B31–B45.

Betcher R.N., Matille G. and Keller G. 2005. Yes Virginia, there are buried valley aquifers in Manitoba. *Proceedings of the 58th Canadian Geotechnical Conference*, 6E-519.

BurVal Working Group. 2009. Buried Quaternary valleys a geophysical approach. *Zeitschrift der Deutschen Gesellschaft für Geowissenschaften* **160**, 237–247.

Crow H.L., Knight R.D., Medioli B.E., Hinton M.J., Plourde A., Pugin A.J.-M., Brewer K.D., Russell H.A.J. and Sharpe D.R. 2012. Geological, hydrogeological, geophysical, and geochemistry data from a cored borehole in the Spiritwood buried valley, southwest Manitoba. Geological Survey of Canada, Open File 7079.

Eberle D.G. and Siemon B. 2006. Identification of buried valleys using the BGR helicopter-borne geophysical system. *Near Surface Geophysics* **4**, 125–133.

Farquharson C.G. and Oldenburg D. W. 1993. Inversion of time-domain electromagnetic data for a horizontally layered Earth. *Geophysical Journal International* **114**, 433–442.

Fountain D. 1998. Airborne electromagnetic systems – 50 years of development. *Exploration Geophysics* **29**, 1–11.

Gabriel G., Kirsch R., Siemon B. and Wiederhold H. 2003. Geophysical investigation of buried Pleistocene subglacial valleys in Northern Germany. *Journal of Applied Geophysics* **53**, 159–180.

Hoyer A.-S., Lykke-Andersen H., Jorgensen F. and Auken E. 2011. Combined interpretation of SkyTEM and high-resolution seismic data. *Physics and Chemistry of the Earth* **36**, 1386–1397.

Huang H. and Rudd J. 2008. Conductivity-depth imaging of helicopter-borne TEM data based on a pseudolayer half-space model. *Geophysics* **73**, F115–F120.

Jørgensen F., Lykke-Andersen H., Sandersen P.B.E., Auken E. and Normark E. 2003. Geophysical investigations of buried Quaternary

valleys in Denmark: An integrated application of transient electromagnetic soundings, reflection seismic surveys and exploratory drillings. *Journal of Applied Geophysics* **53**, 215–228.

Jørgensen F. and Sandersen P.B.E. 2009. Buried Valley mapping in Denmark: Evaluating mapping method constraints and the importance of data density. *Zeitschrift der Deutschen Gesellschaft für Geowissenschaften* **160**, 211–223.

van der Kamp G. and Maathius H. 2012. The unusual and large drawdown response of buried-valley aquifers to pumping. *Ground Water* **50**, 207–215.

Loke M.H., Acworth I. and Dahlin T. 2003. A comparison of smooth and blocky inversion methods in 2D electrical imaging surveys. *Exploration Geophysics* **34**, 182–187.

Macnae J. and Baron-Hay S. 2010. Reprocessing strategy to obtain quantitative early time data from historic VTEM surveys. *ASEG Extended Abstracts*.

Martinez K., Lo B., Ploug C., Pitcher D. and Tishin P. 2008. Water resources applications with the VTEM system. *Proceedings of the 5th International Conference on Airborne Electromagnetics*, 08-01.

Meng Q., Hui H. and Yu Q. 2006. The application of an airborne electromagnetic system in groundwater resource and salinization studies in Jilan, China. *Journal of Environmental and Engineering Geophysics* **11**, 103–109.

Oldenborger G.A. 2010a. AeroTEM III Survey, Spiritwood Valley, Manitoba, parts of NTS 62G/3, 62G/4, Manitoba. Geological Survey of Canada, Open File 6663.

Oldenborger G.A. 2010b. AeroTEM III Survey, Spiritwood Valley, Manitoba, parts of NTS 62G/3, 62G/4, 62G/5, 62G/6, Manitoba. Geological Survey of Canada, Open File 6664.

Oldenborger G.A., Pugin A.J.-M., Hinton M.J., Pullan S.E., Russell H.A.J. and Sharpe D.R. 2010. Airborne time-domain electromagnetic data for mapping and characterization of the Spiritwood Valley aquifer, Manitoba, Canada. Geological Survey of Canada, Current Research, 2010–11.

Oldenborger G.A., Routh P.S. and Knoll M.D. 2007. Model reliability for 3D electrical resistivity tomography: Application of the volume of investigation index to a time-lapse monitoring experiment. *Geophysics* **72**, F167–F175.

Oldenburg D. and Li Y. 1999. Estimating depth of investigation in DC resistivity and IP surveys. *Geophysics* **64**, 403–416.

Palacky G.J. 1988. Resistivity characteristics of geologic targets. In: *Electromagnetic Methods in Applied Geophysics,* Vol. 1 (ed. M.N. Nabighian), pp. 53–129. Society of Exploration Geophysicists.

Palacky G.J. and West G.F. 1991. Airborne electromagnetic methods. In: *Electromagnetic Methods in Applied Geophysics*, Vol. 2 (ed. M.N. Nabighian), pp. 811–880. Society of Exploration Geophysicists.

Paterson N.R. and Bosschart R.A. 1987. Airborne geophysical exploration for ground water. *Ground Water* **25**, 41–50.

Pugin A.J., Oldenborger G.A. and Pullan S.E. 2011. Buried valley imaging using 3-C seismic reflection, electrical resistivity and AEM surveys. *Proceedings of the Symposium on the Application of Geophysics to Environmental and Engineering Problems*, pp. 586–595.

Pugin A.J.-M., Pullan S.E. and Hunter J.A. 2009a. Multicomponent high resolution seismic reflection profiling. *The Leading Edge* **28**, 936–945.

Pugin A.J.-M., Pullan S.E., Hunter J.A. and Oldenborger G.A. 2009b. Hydrogeological prospecting using P- and S-wave landstreamer seismic reflection methods. *Near Surface Geophysics* **7**, 315–327.

Randich P.G. and Kuzniar R.L. 1984. Geology of Towner County, North Dakota. North Dakota State Water Commission, County Groundwater Studies 36, Part III.

Russell H.A.J., Hinton M.J., van der Kamp G. and Sharpe D. 2004. An overview of the architecture, sedimentology and hydrogeology of buried-valley aquifers in Canada. *Proceedings of the 57th Canadian Geotechnical Conference*, pp. 26–33.

Shaver R.B. and Pusc S.W. 1992. Hydraulic barriers in Pleistocene buried-valley aquifers. *Ground Water* **30** 21–28.

Siemon B., Christiansen A.V. and Auken E. 2009. A review of helicopter-borne electromagnetic methods for groundwater exploration. *Near Surface Geophysics* **7**, 629–646.

Smith B.D., Abraham J.D. and Lundstrom S.C. 2010. Airborne electromagnetic surveys by the U.S. Geological Survey over concealed glacial aquifers, central United States: *Proceedings of the Symposium on the Application of Geophysics to Environmental and Engineering Problems*, pp. 126–137.

Smith R.S. and Annan A.P. 2000. Using an induction coil sensor to indirectly measure the B-field response in the bandwidth of the transient electromagnetic method. *Geophysics* **65**, 1489–1494.

Smith R.S., O'Connell M.D. and Poulsen L.H. 2004. Using airborne electromagnetics surveys to investigate the hydrogeology of an area near Nyborg, Denmark. *Near Surface Geophysics* **3**, 123–130.

Sørensen K.I. and Auken E. 2004. SkyTEM – A new high-resolution helicopter transient electromagnetic system. *Exploration Geophysics* **35**, 191–199.

Steuer A., Siemon B. and Auken E. 2009. A comparison of helicopter-borne electromagnetics in frequency- and time-domain at the Cuxhaven valley in Northern Germany. *Journal of Applied Geophysics* **67**, 194–205.

Walker S. and Rudd J. 2008. Airborne resistivity mapping with helicopter TEM: An oil sands case study. *Proceedings of the 5th International Conference on Airborne Electromagnetics*, 06-03.

West G.F., Macnae J.C. and Lamontagne Y. 1984. A time-domain EM system measuring the step response of the ground. *Geophysics* **49**, 1010–1026.

Wiecek S. 2009. Municipality of Killarney, Turtle Mountain groundwater assessment study. W.L. Gibbons & Associates Inc.

Winter T.C., Benson R.D., Engberg R.A., Wiche G.J., Emerson D.G., Crosby O.A. and Miller J.E. 1984. Synopsis of ground-water and surface-water resources of North Dakota. United States Geological Survey, Open File Report 84-732.

Wynn J., Bultman M. and Lemieux J. 2005. Airborne geophysics versus groundwater – An example. In: *Near-Surface Geophysics* (ed. D.K. Butler), pp. 635–641. Society of Exploration Geophysicists.